17èmes JOURNEES DE L'HYDRODYNAMIQUE
JH2020

24 - 26 novembre 2020
CHERBOURG - en - COTENTIN

Validation of actuator line method in mesoscale solver Meso-NH - Comparison with field measurements in wake

17emes JOURNEES DE L'HYDRODYNAMIQUE JH2020

E. Jézéquel[(1),(2)*], M. Cathelain[(1)], and V. Masson[(2)]

[(1)]IFP Energies nouvelles, France
[(2)]Centre National de Recherches Météorologiques, France
[*]Corresponding author: erwan.jezequel@ifpen.fr

Résumé

Le sillage derrière une éolienne est caractérisé par une diminution de la vitesse de vent et une augmentation de l'intensité turbulente comparée à l'écoulement en amont. Dans un parc éolien, cela impacte les éoliennes situées en aval (en termes de puissance produite, chargement et fatigue). La longueur du sillage (environ 10 à 15 fois le diamètre de l'éolienne) dépend de nombreux paramètres, en particulier de la stabilité atmosphérique, de la force de Coriolis, du forçage des grandes échelles ou de l'orographie. Pour simuler cette interaction, la méthode de ligne actuatrice (ALM) a été développée dans le code atmosphérique Meso-NH (code LES développé par le Centre National de Recherches Météorologiques - CNRM). Cette implémentation a déjà été validée pour le chargement des pales sur le cas de soufflerie Mexico (avec un écoulement uniforme) et pour les interactions avec l'atmosphère sur le cas du parc de Horns Rev. Le travail présenté ici vise à compléter cette validation en se focalisant sur les propriétés et l'évolution du sillage. Il repose sur le benchmark international SWiFT qui compare les résultats de nombreux codes numériques avec des mesures LiDAR d'un sillage d'une éolienne unique dans les grandes plaines des Etats-Unis.

Summary

The wake behind a wind turbine is characterised by a decrease of wind velocity and an enhanced turbulence intensity compared to the inflow properties. In wind farms, it has an impact on the turbines located downstream (in terms of power production, loads, and fatigue). The wake length (approximately 10-15 times the diameter of the turbine) depends on many parameters such as the stratification, Coriolis force, large scale forcing and orography. The actuator line method (ALM) has been developed in the atmospheric code Meso-NH (LES research code developed by the French weather services) to simulate this interdependence. This implementation has already been validated for loading of the blade on the Mexico case (uniform inflow in a wind tunnel) and for the interaction with the atmosphere on the Horns Rev case. The work presented herein aims to complete the validation with a focus on the wake properties. It is based on the international SWiFT benchmark which compares the results of many numerical codes with LiDAR measurements in the wake of a single turbine located in the great plains in the United States.

1. Introduction

The wake behind a wind turbine is characterised by a decrease of wind velocity and an enhanced turbulence intensity compared to the inflow properties. On one hand, the upstream wind turbine extracts momentum from the free flow, i.e. 'slowing it down'. The velocity deficit in the wake gradually diminishes due to turbulent mixing, however this wake recovery can extend up to 10-15 diameters and thus the downstream wind turbines might be placed in the perturbed region. As a result, production losses (10% to 20% [1]) due to wake effects arise for downstream wind turbines [2]. On the other hand, several phenomena increase the turbulence level in the wake, namely: the blade bound vorticity (i.e. tip and root vortices breaking down), the wake-generated shear and the wake meandering [3]. The turbulence increase arising from these phenomena changes drastically the structural loading and fatigue of the blades, leading to a reduction of the wind turbine's life expectancy.

Industrials usually aim at assessing and optimizing the annual energy production as well as the lifespan of their turbines, and thus need to investigate all the potential wind directions, velocities and atmospheric conditions that may arise at the given site and their impact on the farm. In order to do so, a lot of simulations are necessary, and it is unreasonable to use large eddy simulations (LES) because of the high computational cost. Instead, engineering tools such as FarmShadow™ (developed by IFPEN) or WindFarmer:Analyst [4] are used.

As the turbines are getting larger and larger (e.g the diameter of the reference turbine DTU 10MW is 180m), the flow cannot be considered uniform on the rotor area: ground-generated shear and Coriolis-generated veer must be taken into account. Moreover, the height of very large turbines might coincide with the atmospheric boundary layer (ABL) height in offshore locations [5]. Finally, phenomena such as wake meandering are driven by atmospheric forcing [6] and the atmospheric stability influences the recovery of the wakes [7].

It is thus important to account for the effects of the ABL when simulating wind turbines and wind farms. In the present work, high-fidelity computations are used with the meso-scale meteorological LES solver Meso-NH [8]. This solver developed by both Météo-France and Laboratoire d'Aérologie takes into account the main meteorological phenomena of interest (Coriolis forces, stability of the ABL, the diversity of eddies scales in the atmosphere...). It can also model other effects likely to interact with wind turbines such as complex terrain, precipitations, clouds, sea-air and coupling. Wind turbines are modelled in Meso-NH through an actuator line method (ALM) which has proven its capacity to resolve correctly the blades loading and the impact on the atmosphere [5]. In the work presented hereby, this validation is completed with a focus on wind turbine wakes. It is encompassed in a Ph. D. which aims to add physic insight in the FarmShadow^{TM} model by calibration with Meso-NH.

In order to validate the ability of the code to represent a realistic wake, the case of the SWiFT set-up [9] is studied, which is a benchmark of a stand-alone turbine's wake over a flat terrain. There are three cases with different atmospheric stability regimes (stable, neutral, unstable). Reference data come from a meteorological mast for the inflow, and LiDAR (Light Detection And Regime) measurements for the wake. Different codes used in the wind turbine community, with different degrees of fidelity are compared based on these field results: LES (SOWFA, PALM, EllipSys3D), RANS (EllipSys3D), and engineering models (FAST.Farm, FarmShadow^{TM}, FLORIS).

2. Presentation of the model

To study numerically the ABL, the highest fidelity method available in modern high performance computers (HPC) are the LES, as done in Meso-NH (see Section 2.1). The principle of LES is to use a high-pass filter on the Navier-Stokes equations. The largest eddies of the flow are resolved by the filtered equations and the smallest ones are modelled through a subgrid term, added in the equations. The cut-off wavelength of this

filter is proportional to the grid size. A LES is considered to be valid if 20% or less of the turbulent kinetic energy (TKE) is resolved; otherwise, the result of the simulation will vary too much with the subgrid model.

To model a wind turbine in a LES code, it is not reasonable to resolve the boundary layer over the turbine's blade because the scales involved are much smaller than those in the ABL. Instead, it is popular to use an actuator method [5, 10, 11] such as the ALM. The principle is to add body forces (i.e momentum sources) in the governing equations of the flow to model the efforts of the blades over the flowfield.

2.1 The Meso-NH model

Meso-NH (MESOscale Non Hydrostatic) is an open-source research code for ABL simulations developed by Centre National de Recherches Météorologiques (CNRM) and Laboratoire d'Aérologie. The first version of the model is presented in Lafore et al. [12], and recent updates are shown in Lac et al. [8]. It can deal with scales ranging from synoptic (hundreds of kilometers) to micro-scale (around a meter). The mesh generator can take into account complex terrain (orography) and several physical schemes allow to represent phenomena such as clouds and precipitation. Moreover it can be coupled with chemical or surface schemes, leading to a broad variety of capabilities ranging from cyclones to urban heat island predictions (a list of applications is given in [8]). The code is parallelised in order to run on HPC. The unknowns of the system are the velocities (U_x,U_y and U_z) and the potential temperature ($\theta = T(1/P)^{0.286}$ with T the temperature and P the pressure in bar). The equations are similar to the incompressible Navier-Stokes equations (i.e elliptic pressure equation), with the following differences:

- The Boussinesq hypothesis is used: the equations use a constant density ρ, but a buoyancy term is added to the momentum equation.
- The equations are non-hydrostatic: the vertical pressure gradient term is not simplified with the gravity term.
- The Coriolis term is added to the momentum equation to take into account the rotation of the earth: $\overrightarrow{f_{Cor}} = 2\overrightarrow{\Omega}_E \wedge \overrightarrow{U}$ (where $\overrightarrow{\Omega}_E$ is the rotation vector of the Earth).
- The momentum equation is modified to take into account large-scale forcing (the horizontal synoptic pressure gradient, which cannot be naturally taken into account in too small domains): $\overrightarrow{f}_{geos} = -2\overrightarrow{\Omega}_E \wedge \overrightarrow{U}_{frc}$; where $\overrightarrow{U}_{frc}$ is called the geostrophic wind and is defined by the user.

As in any LES code, the filtered Navier Stokes set of equations has more unknowns than equations because of additional terms called turbulent fluxes: $\overline{\theta' u'_j}$ and $\overline{u'_i u'_j}$ (where the overbar and the prime denote respectively the mean and fluctuating parts of the Reynolds decomposition). In Meso-NH, the set of equations is closed by solving an additional equation for the turbulent kinetic energy (TKE, or $e = 0.5\overline{u'_i u'_i}$) and by relating the turbulent fluxes and e to a mixing length written $\mathscr{L}$. This parameter, defined by the user, can be linked to the size at which the eddies are resolved. For LES cases (3D turbulence), the mixing length is directly related to the mesh size: $\mathscr{L} = \sqrt[3]{\Delta X \Delta Y \Delta Z}$, with a modification to take into account stratification (this is known as the Deardorff formulation [13]).

The set of equations is solved on an Arakawa grid: the velocity variables are positioned on the face of each cell whereas the scalar variables (temperature, subgrid TKE...) take place at the centre of the cells. The numerical schemes used for this work are: a centered scheme of fourth order for transport and Runge-Kunta fourth order scheme for time integration. This leads to an accuracy of $4\Delta X$ [8] (i.e the smallest resolved turbulent structures will be at best of four time the mesh size).

The model is initialised with horizontally constant profiles of velocity, temperature and moisture. Then, a perturbation field is set, either on the vertical component of the velocity or on the temperature field. This perturbation allows the creation of turbulent eddies much faster than if it had to naturally develop.

Finally, Meso-NH has the capacity to perform grid nesting [14]: it allows to resolve a limited part of the computational domain (for instance, the wind turbine's wake region) with an higher spatial resolution. The idea is to compute in parallel two models, a large one with a relatively coarse mesh (CM) and a smaller one with a finer mesh (FM) and to use the field of CM as the boundary conditions of FM. In Meso-NH, the grid nesting is only available in the horizontal directions (the vertical mesh for CM and FM is the same). The mesh size ratio must be an integer lower or equal to 5, and a different time step can be applied to both models (to fulfill the Courant-Friedrichs-Lewy condition in all models).

2.2 The actuator line method

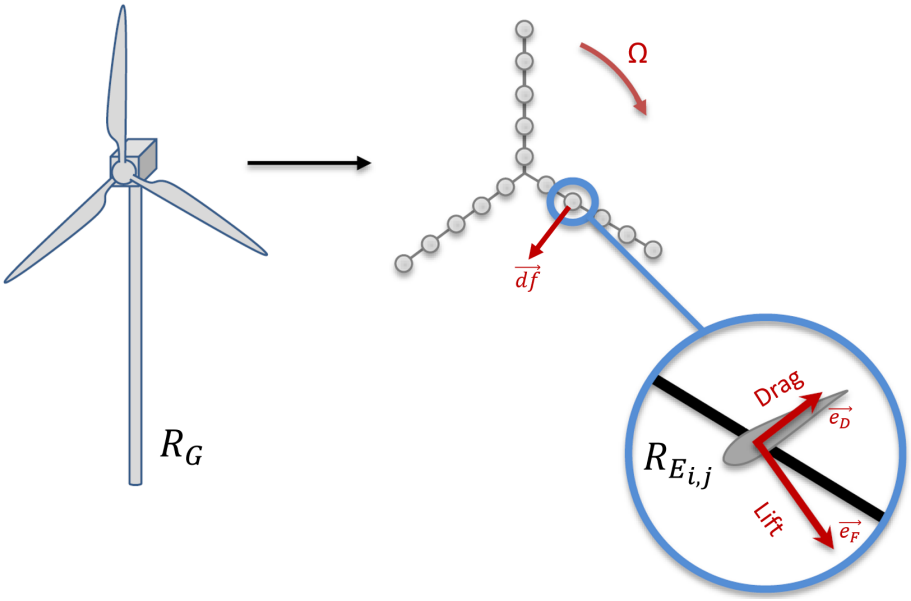

Figure 1. The actuator line method in Meso-NH, scheme from [15].

In the ALM, the wind turbine blades are modelled by a line of body forces, i.e momentum source terms added to the momentum equation. Blade element momentum (BEM) theory [16] and tabulation in airfoil data of each blades allow to compute the values of the body forces. Let the rotor's cylindrical coordinate system be called (r,θ,z). c is the chord of the airfoil, U_{rel} is the 2D local relative velocity of the wind at an airfoil. C_L and C_D are the lift and drag coefficients (and their respective unit vector are written $\overrightarrow{e_L}$ and $\overrightarrow{e_D}$), given in airfoil tables as a function of the angle of attack α and the Reynolds number Re. The angle of attack is deduced from $\alpha = \phi - \gamma$ where $\gamma(r)$ is the local pitch angle (sum of the pitch of the blade and the twist) and $\phi = tan^{-1}(U_z/(\Omega r - U_\theta))$ is the angle between the relative velocity and the rotor plane. The force induced by the turbine per spanwise unit length can be written [17]:

$$\overrightarrow{df} = \frac{1}{2}\rho U_{rel}^2 c(C_L\overrightarrow{e_L} + C_D\overrightarrow{e_D}) \qquad (1) \qquad\qquad \overrightarrow{U_{rel}} = \left(U_\theta - \Omega r; U_z\right) \qquad (2)$$

The last step is to extract the velocity $\overrightarrow{U_{rel}}$ from the Meso-NH flow field and to deduce the orientation of each airfoil ($\overrightarrow{e_L}$ and $\overrightarrow{e_L}$) from the blade position. The implementation of the ALM in Meso-NH during the preceding Ph. D. [18, 15] is schemed in Figure 1. Instead of computing directly the relative velocity, it has been preferred to build one coordinate system for each part of the turbine plus one "global" which corresponds to the Meso-NH domain. They are called R_G, R_T, R_N, R_H, R_{B_i} and $R_{E_{i,j}}$ respectively for the global, tower, nacelle, hub, blade i and element j of the blade i. The transfer matrix M between each coordinate system is computed at every time step. Once these matrices are known, the computation of relative velocities is easier:

$$\overrightarrow{U^{ij}_{rel}}|_{R_{E_{ij}}} = M_{R_{E_{ij}} \longrightarrow R_{G_{ij}}} \cdot \overrightarrow{U^{ij}_{vent}}|_{R_{G_{ij}}} - \overrightarrow{U^{ij}_{trans}}|_{R_{E_{ij}}} \quad (3)$$

$$\alpha = tan^{-1}\left(\frac{\overrightarrow{U^{ij}_{rel}}|_{R_{E_{ij}}} \cdot \overrightarrow{x}}{\overrightarrow{U^{ij}_{rel}}|_{R_{E_{ij}}} \cdot \overrightarrow{y}}\right) \quad (4)$$

where $\overrightarrow{U^{ij}_{trans}}|_{R_{E_{ij}}}$ is the translation velocity, equal to $\overrightarrow{0}$ if the tower is not moving. The elementary forces can be computed with:

$$dF_L = \frac{1}{2} C_L \rho c U^2_{rel} dr \quad (5) \qquad dF_D = \frac{1}{2} C_D \rho c U^2_{rel} dr. \quad (6)$$

C_L and C_D are deduced from cubic interpolation of tabulated data of the different airfoils composing the blades. These forces must be rotated by an angle of α and put in the global frame (multiplication by $M_{R_{G_{ij}} \longrightarrow R_{E_{ij}}}$). The computed values of the forces are then inserted as source terms in the Meso-NH at the current position of the blades. It is possible to smear the resulting forces with different functions (linear or gaussian kernel). In Equation 1, U_{rel} is computed with the interpolation of eight neighbouring cells (again, to smooth the resulting forces). The drag forces of the nacelle and the tower are implemented as the drag of a cylinder (with the wind coming from the side for the tower and from the top for the nacelle), with $C'_{nacelle} = 4$ and $C'_{tower} = 0.68$ [19]:

$$F_{nacelle} = -\rho \frac{1}{2} C'_{nacelle} U^2_{nacelle} \frac{\pi}{4} D^2_{nacelle}. \quad (7) \qquad F_{tower} = -\rho \frac{1}{2} C'_{tower} U^2_{tower} D_{tower} z_h. \quad (8)$$

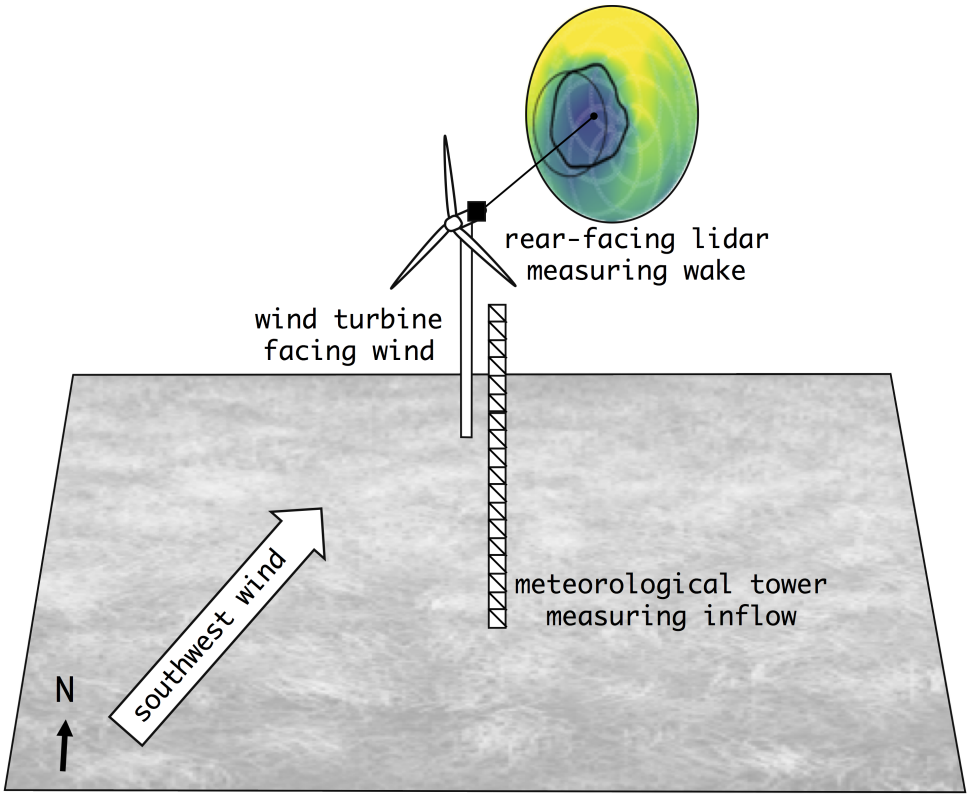

Figure 2. Schematic of the part of the SWiFT facility used for this benchmark.

3. Workflow

3.1 The SWiFT Case

SWiFT (Scaled Wind Farm Technology) is a facility funded by the United States (U.S) Department of Energy, operated by Sandia National Laboratories as well as National Renewable Energy Laboratory (NREL), and hosted at Texas Tech University's National Wind Institute Research Center in Lubbock, Texas. The SWiFT site is located in the U.S. Great Plains and is therefore exempt from complex, terrain-induced flow patterns. In the absence of weather phenomena, the atmospheric conditions at the SWiFT site approximate canonical diurnal cycles: the characteristics of wakes can be measured without the influence of complex terrain and weather [20].

The NREL has organised an exercise of international code intercomparison based on this facility, called hereafter "SWiFT benchmark". It compares different types of codes (such as low-fidelity 2D steady state, mid-fidelity RANS and high-fidelity LES) from different institutions around the world (NREL, DTU, IFPEN, ForWind). The results have been published in 2020 [9]. This benchmark aims at comparing the capacity of the different codes to reproduce the wake of a single wind turbine in an atmospheric inflow. The turbine is a classical 3-bladed horizontal axis wind turbine of diameter $D = 27$m and $z_{hub} = 32.1$m. A LiDAR mounted on the nacelle measures the wake at different locations downstream, and a meteorological mast measures the inflow conditions. A scheme of the disposition is available in Figure 2.

The SWiFT benchmark is separated in three cases of stability: neutral, stable and unstable. This work focuses on the reproduction of the neutral case (the influence of heat flux is negligible), which is the first step toward reproducing unstable and stable cases. For the neutral case, the inflow conditions are given on Table 1.

Variable	Notation	Value	Height measurement
Velocity at hub height	$\overline{U_\infty}$	8.7m/s	32.1m
Turbulence intensity at hub height	TI	10.7%	32.1m
Roughness length range	z_0	$0.005 - 0.05$m	-
Friction velocity	u_*	0.08m/s	10m
Stability parameter	$\xi = z/L_{MO}$	0.004	10m
Kinematic vertical heat flux	$\overline{w'\theta'}$	-0.002K.m/s	10m

Table 1. Inflow conditions measured by the meteorological mast.

3.2 Methodology

The SWiFT benchmark is decomposed in three steps:

- Firstly, it is necessary to reproduce the inflow conditions with fidelity. The inflow conditions in the SWiFT benchmark are measured with the meteorological mast (variables are summed up in Table 1), approximately placed $2.5D$ (65m) upstream (for southwest wind: the direction chosen for the benchmark). In the simulations, it corresponds to the mean values in a plane 65m upstream the turbine, averaged in the spanwise direction. In the original publication [9], five criteria are examined to validate the inflow: mean horizontal wind speed profile, mean wind direction, turbulent kinetic energy, and spectrum of the u and v quantities. In order to have comparable outputs, modellers were asked to provide the 10 minutes series of U_x, U_y and U_z, at a frequency of 1Hz. Consequently, the TKE profile does not take into account the subgrid quantities and only the contribution of eddies of frequency comprised between 1.67×10^{-3}Hz ($= 1/10$min) and 1Hz. Likewise, spectra can only be computed on this range.

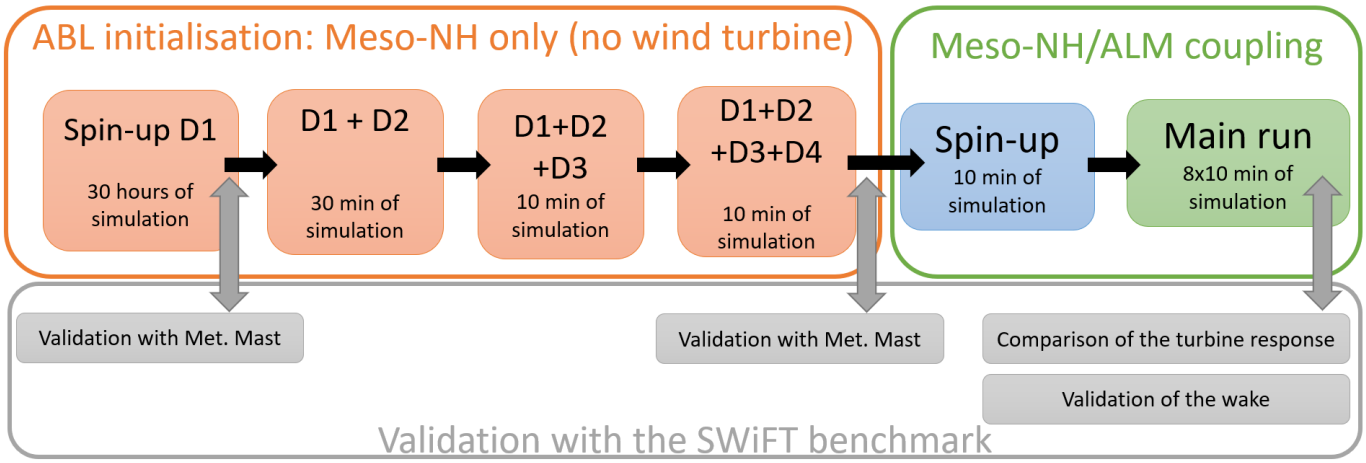

Figure 3. Flowchart of the methodology of the presented work.

- Secondly, the wind turbine response is evaluated. Four variables are used in the original publication: the output thrust coefficient, power, torque, and rotational speed. In this work, the rotational speed is fixed to the value corresponding to the output of the controller (4.56rad/s) for the benchmark velocity at hub height, and is not changed (some other models use a "true" controller which modifies the turbine rotational speed live). Consequently, only the mean thrust coefficient $\overline{C_T}$ and the mean generator power $\overline{P_{gen}}$ are studied herein because torque and rotational speed become redundant. Note also that no thrust measurement were available on the turbine and thus $\overline{C_T}$ is only compared against other models.

- Finally, the velocity deficit in the wake is computed using the velocity in the inflow plane (thereafter noted $\overline{U_\infty}$) as a reference. The results are plotted as a function of the spanwise (y) variable.

Reaching a given inflow condition with Meso-NH is however not an easy task: the user cannot prescribe directly a given profile of wind speed or TKE. Instead, he must use the geostrophic wind, the initial conditions and the ground forcing ($\overline{w'\theta'}$, z_0, u_*) in order to reach the desired inflow profile. Four nested models are used here (the reason is further explained in Section 4.1), and the profiles need to be accurate in the last domain, where the wind turbine will be placed. Once this is done, the wind turbine is placed in the flow. The first ten minutes of dynamics of the turbine are not used ("spin-up") in order to let the wake flow develop and then the results of eight segments of ten minutes each are averaged (as it is done in the original publication [9]). The whole workflow followed in this work is described in Figure 3: the first step of the list described above corresponds to the orange box whereas the second and third parts are in the green box. The different validations appear in grey: the two first (respectively for domains D_1 and D_4) correspond to the first step of the list above whereas the two on the right correspond to the second and third steps.

4. Numerical set-up

4.1 Numerical parameters

In a neutral ABL, the potential temperature is constant with height. Above, a region of strong gradient called inversion zone defines the height of the boundary layer z_i. In Meso-NH, this inversion zone is defined by imposing a vertical temperature profile in the initial conditions. In this case, we set the arbitrary value of $z_i = 1000$m (a canonical value for neutral ABL) since no field value is given in the benchmark. Consequently, the vertical mesh extends up to 2000m, with a "sponge" zone at 1500m to absorb wave reflection from the top boundary condition. The grid size is $\Delta Z = 0.5$m near the ground and stretches to the size of 50m above the rotor-swept region (46m).

The horizontal domain size must approximately be a couple of time the size of the largest eddies of the flow to let them develop before reaching the cyclic boundary conditions. In the case of neutral atmosphere,

these eddies are of the order of magnitude of z_i. The domain size is thus fixed at $L_X = 6$km and $L_Y = 2.4$km. On the other hand, the literature recommends at least 20 cells per blades for the ALM. A resolution of 0.5m allows to have between 27 and 19 cells per blades. Creating the directly the mesh is too expensive so three consecutive grid-nestings are used here. It result into four domains, respectively noted D_1, D_2, D_3 and D_4, which parameters are reported in Table 2.

Parameter	D_1	D_2	D_3	D_4
ΔZ [m]	0.5			
ΔX=ΔY [m]	20	4	1	0.5
L_X [m]	6400	2000	600	432
L_Y [m]	2400	800	240	162
Δt [s]	0.2	0.1	0.05	0.025
Mixing length	Deardorff			
Numerical Diffusion [s]	600	120	30	15
Spatial scheme	4th order centered			
Temporal scheme	Runge-Kutta 4th order			

Table 2. Numerical parameters of the different domains.

For the ALM parametrisation, each line is composed of 40 body forces. The Glauert correction for tip loss is used [5]. With a timestep of $\Delta t = 0.025$s (see Table 2), the tip of the blades crosses around three cells at each timestep. This is known to be a source of error and to correct it, a time splitting method has been implemented in Meso-NH[5]: in this case, at each timestep of the D_4 domain, the ALM does three sub-steps (one on each crossed cells). We use a linear function to smear the resulting body forces in the Meso-NH field.

4.2 Spectral study

When nesting a domain D_i into a domain D_{i-1}, there is a region in D_i (near the inlet) where the turbulent structures are still at the D_{i-1} scale, and are progressively scaling down to the size of D_i. In order to have a resolution corresponding to the actual mesh size (around $4\Delta X$ for this spatial scheme), one needs to be outside of this turbulence build-up region. Thus, the domain D_{i+1} (or the turbine, if $i = 4$) must be placed downstream the build-up region. This region can be seen with the naked eye (Figure 4a), however we propose a more quantitative approach: some probes are located at various distances to the inlet in the D_i domain. Once a neat (and "converged") cut-off frequency in the power-spectral density is seen, the build-up region is considered to be finished.

This is illustrated for $i = 2$ in Figure 4. Near the inlet boundary (blue curve) of the domain, the flow has not a clear cut-off at the frequency ($f \simeq 0.55$Hz) corresponding to the domain's spatial resolution (4m). From Figure 4b, one can see that the cut-off frequency of domain D_1 ($f \simeq 0.1$Hz) has still a large influence on the flow field at this location. This influence reduces progressively with the distance from the inlet, and the three last probes (green, red and purple) measure a similar spectrum with a neat cut-off frequency and follow correctly the canonical slope of the Kolmogorov cascade (dashed black line) for $f \leq 0.55$Hz. It is thus decided to place the next nested domain D_3 at least after the green probe (black box in Fig4a). This methodology is then applied on domain D_3 and D_4 in order to have a correct turbulence cascade 65m upstream the wind turbine. The build-up distance is smaller for D_3 and D_4, probably because the mesh size and refinement ratio (respectively 4 and 2) is smaller than for D_2 (refinement ratio is 5).

5. Results

This section presents the results of the simulation, compared to the SWiFT benchmark. The benchmark data can be decomposed in field measurements (in black dashed line) and numerical codes (in colours). For the

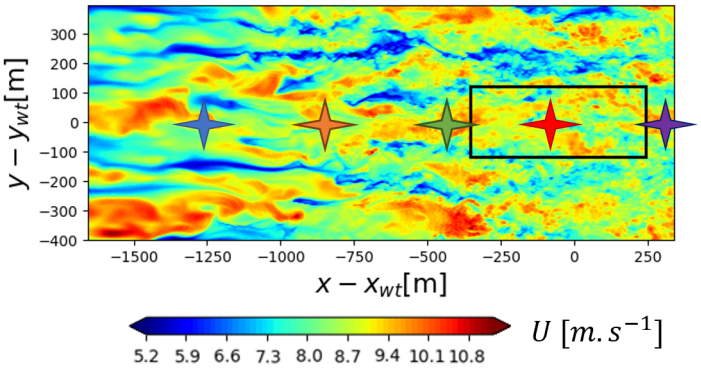

(a) Instantaneous velocity profile at hub height in domain D_2. The stars correspond to the location of the different spectra plotted in Figure 4b. The black box represents the chosen location for the domain D_3.

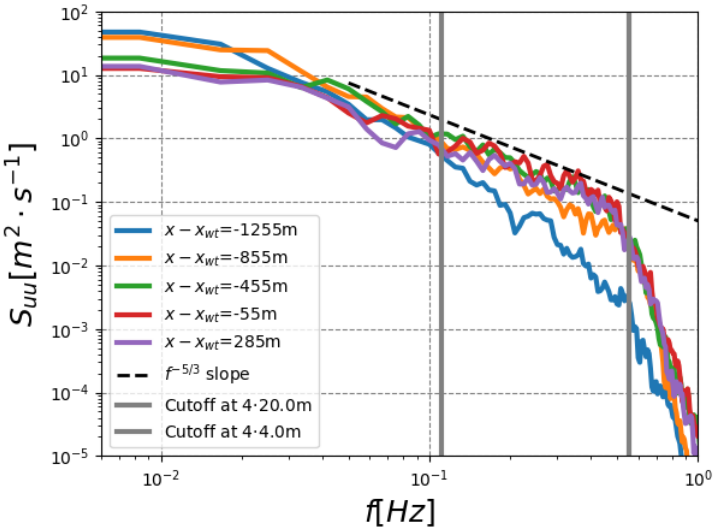

(b) Axial velocity power spectral density at different locations downstream the inlet of domain D_2.

Figure 4. Evolution of the axial velocity spectrum with downstream distance in D_2.

sake of clarity, not all the numerical codes used in the benchmark are represented herein. The original figures as well as a description of each code can be found in the corresponding paper [9]. The experimental data corresponds to six sets of 10 minutes data (described in [21]) but not all of them are always plotted here (at least the maximum and minimum ones). The most important data for the validation of Meso-NH are the experimental data and the LES codes (EllipSys-3D, SOWFA, SOWFA2, NaluWind and PALM), with a special care to PALM, which is the German equivalent of Meso-NH (meteorological code). The main difference between the two is the turbine implementation (coupling with the aero-hydro-servo-elastic code OpenFAST for PALM and classic ALM for Meso-NH).

The post-processing of the results are done in Meso-NH exactly as it has been done in the SWiFT benchmark: in domain D_4, the velocity field of five planes (at $x - x_{wt} = [-65\text{m}, 2D, 3D, 4D, 5D]$) is extracted from the simulation, at a frequency of 1Hz, during 10min. Figures 5, 6 and 8 are post-processed from these fields. Since the Meso-NH simulation lasted 80 minutes, eight samples are averaged over 10 minutes. Note that for the TKE, this excludes the *inter* part of the variance (i.e, the large scale turbulence), and that the subgrid and high frequency ($f > 1$Hz) part are excluded as well in order to have the same sampling frequency than the LiDAR.

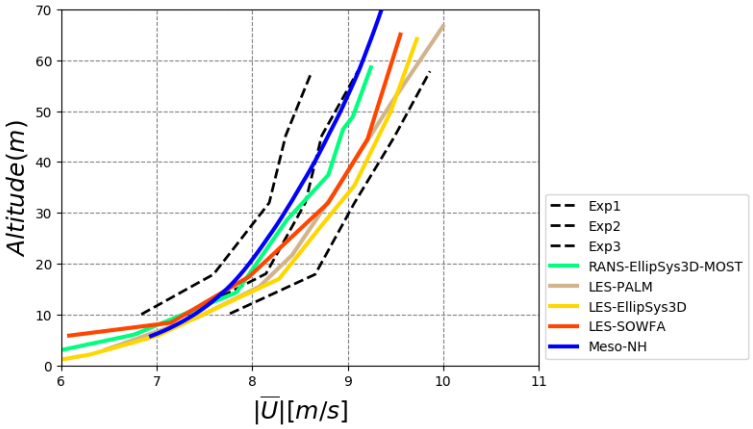

(a) Mean horizontal wind magnitude profile.

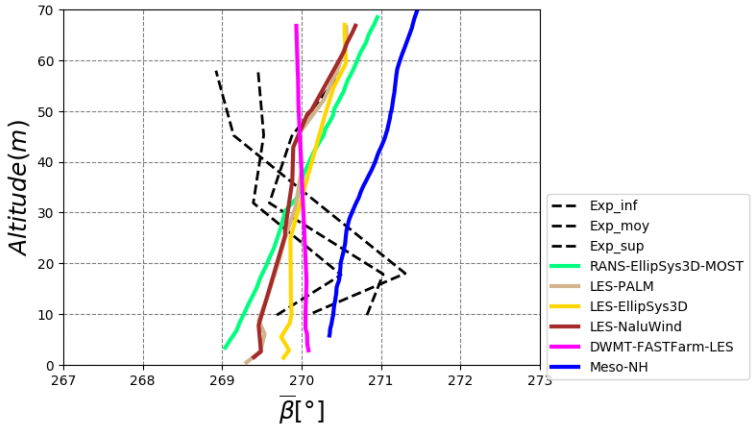

(b) Mean wind direction profile.

Figure 5. Mean inflow velocity (65m upstream the wind turbine), Y-averaged.

5.1 Inflow

The inflow conditions can be decomposed into the mean (Figure 5) and the turbulent (Figure 6) parts of the wind. The mean wind gives overall satisfying results: the horizontal wind magnitude (Figure 5a) is in the range of the experimental data, and slightly lower than the other LES codes. About the wind direction, there is a small yaw at hub height (less than 1°, see Figure 5b). As observed in the original publication, the meteorological mast did not measure a veer in the direction of the Ekman spiral.

Compared to other LES codes (in particular SOWFA and NaluWind), Meso-NH overestimates the turbulent kinetic energy (Figure 6a), but compared to experimental measurements, the performance can be considered satisfying. The streamwise (Figure 6b) and spanwise (not shown here) velocity spectra are very satisfying for Meso-NH, which can be explained from the special care taken to the turbulence during the different nesting steps (Section 4.2).

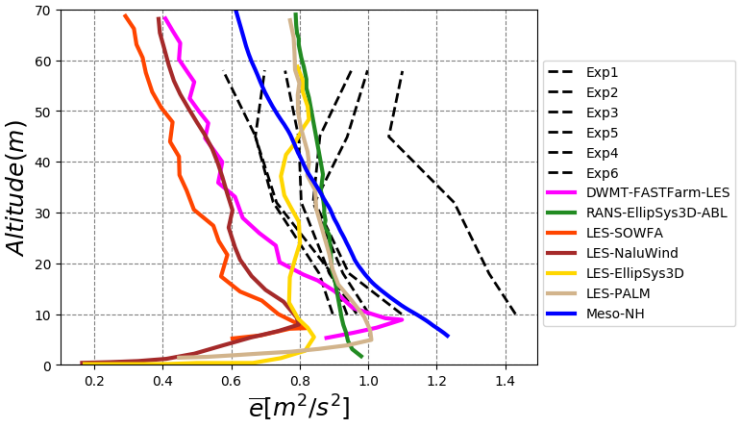

(a) Mean horizontal TKE profile

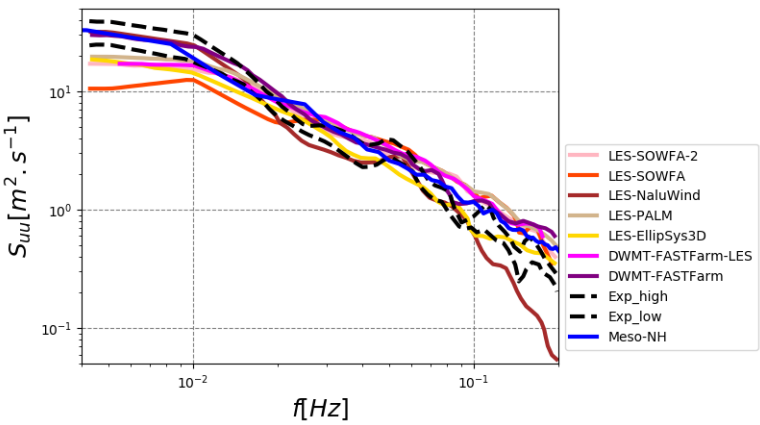

(b) Streamwise velocity spectrum at hub height

Figure 6. Mean inflow turbulence (65m upstream the wind turbine), Y-averaged.

5.2 Turbine response

Since the wind turbine in Meso-NH is rotating at a fixed value, it is redundant to look at both the power and the torque outputs. Consequently, only the thrust coefficient $\overline{C_T}$ and the generator's power output $\overline{P_{gen}}$ are shown here. Results are plotted respectively in Figure 7a and Figure 7b: the mean value corresponds to the magnitude of the colour bar and the standard deviation is represented by the black line on each bar. The measured power on the turbine is reported as the dashed line in Figure 7b. Overall, Meso-NH overestimates the efforts (both tangential and normal), leading to an overestimation of both $\overline{C_T}$ and $\overline{P_{gen}}$. Note that the overestimation is less pronounced for the thrust coefficient, which can be due to a better approximation of the thrust but as well could come from the fact that the value is dimensionless. This is hard to tell because we have no access to the raw values of the benchmark.

There are doubts that these discrepancies come from the inflow conditions, which are quite satisfying. For instance, Figure 5a shows that the velocity is stronger in EllipSys-3D (yellow curve) than Meso-NH, but the power output of this code is about 40% lower. Instead, the two main sources of error could be the projection of the effort in Meso-NH (here, a linear smearing) and the use of time splitting. To investigate the effect of the smearing technique, a Gaussian projection will be used in near future for comparison. The time splitting has already been proven to overestimate the efforts [5] (however in much lower magnitude than what is observed here). Furthermore, the time-splitting validation has been done in a uniform flow (in the Mexico wind tunnel), which is not the case here: the main assumption of the time splitting (that the wind is frozen during the ALM substeps) is not fulfilled in a turbulent flow such as the one for this SWiFT case.

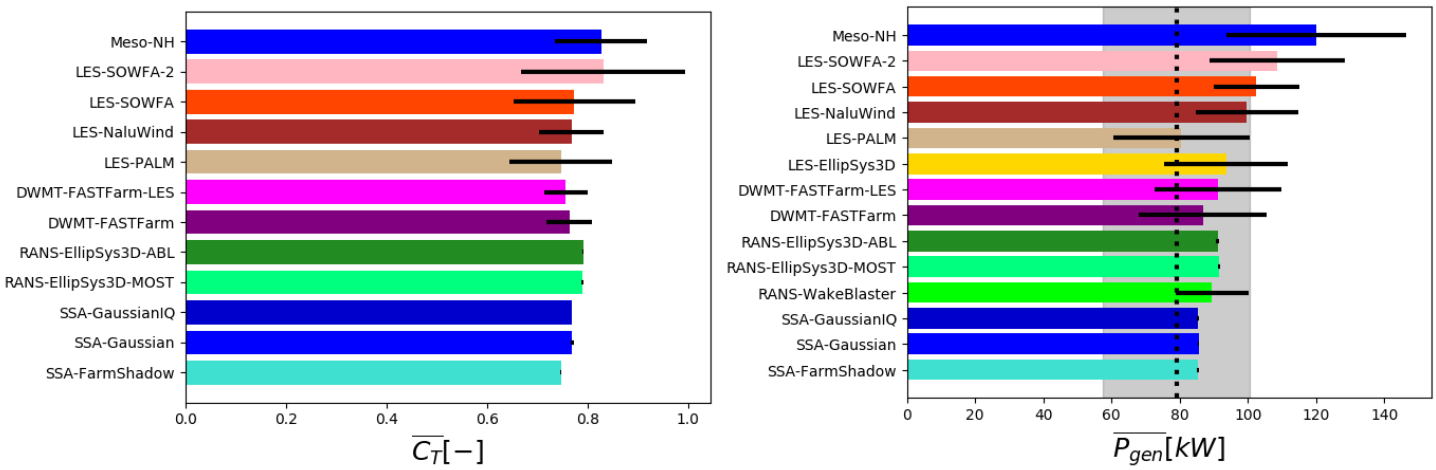

(a) Thrust coefficient.

(b) Power output of the generator.

Figure 7. Mean turbine response.

5.3 Wake

The spanwise distribution of the mean velocity deficit behind the wind turbine (at $2D$, $3D$, $4D$ and $5D$ downstream) are plotted in Figure 8, against the distribution of the LiDAR measurement and the mean of the other LES codes. $\overline{U}_\infty$ denotes the time-averaged value of the velocity field in the inflow plane (65m upstream). It is important to note that the LES codes of the benchmark were, in average, underestimating the wake strength as well as the wake recovery compared to field measurements [9]. Meso-NH simulations show a wake recovery more consistent with the measurements and a wake deficit at $2D$ closer to the measurements as well.

The wake recovery can be linked to the ambient turbulence, which is consistent here since Meso-NH shows values closer to measurements than the average of the other LES (Figure 6a). Likewise, since the efforts in Meso-NH are overestimated compared to the other LES (and especially the thrust coefficient in Figure 7a, which is the main factor for wake strength), it is normal that the wake is stronger in Meso-NH. As a conclusion, the wake in Meso-NH shows slight differences with other LES codes, which are however consistent with the differences observed in the efforts.

6. Conclusions, discussion and perspective

The wakes generated by the coupling of the Meso-NH code with the ALM has been validated here for a realistic near-neutral inflow. To do so, we followed the three steps described in Section 3.2: first, the inflow conditions of the SWiFT benchmark were reconstituted with a good accuracy but Meso-NH, with the configuration used here, overestimated the efforts. This is attributed to the time splitting and smearing techniques in our configuration of the ALM. However, the differences with other LES codes observed in the last step (wakes) are consistent with the efforts (overestimated) and TKE (overestimated as well) differences: thus it is expected that if the efforts are improved (by using more CPU-expensive techniques for the ALM), the wake would be of good quality. Meso-NH is thus able to generate wind turbine wakes which are consistent with the inflow and the turbine efforts.

As a perspective, additional simulations without time splitting and with other smearing techniques could be used to improve the wind turbine loading. The stable and unstable cases will also be simulated with Meso-NH to validate the capacity of the code to represent the effect of stability. Finally, the velocity spectrum inside the wind turbine wake will be investigated, in order to gain insight on the nature of the added turbulence in the wake and to be able to improve engineering models.

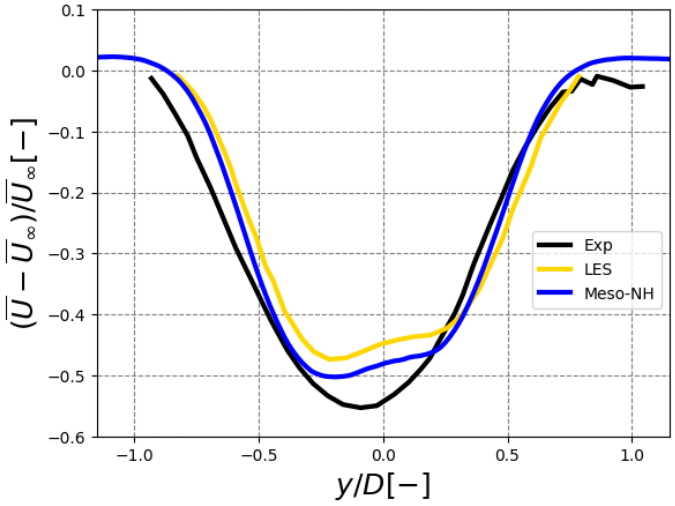

(a) Deficit at 2D downstream the wind turbine

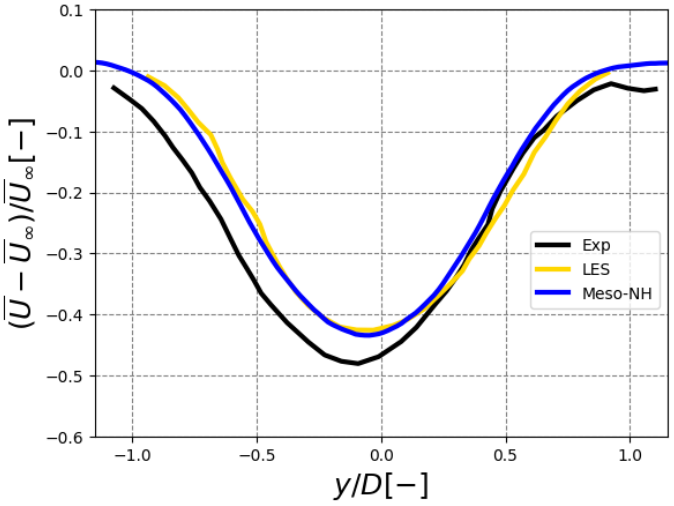

(b) Deficit at 3D downstream the wind turbine

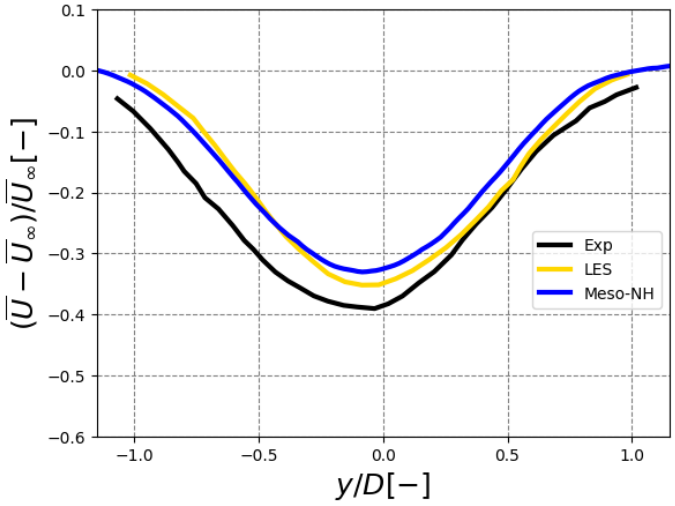

(c) Deficit at 4D downstream the wind turbine

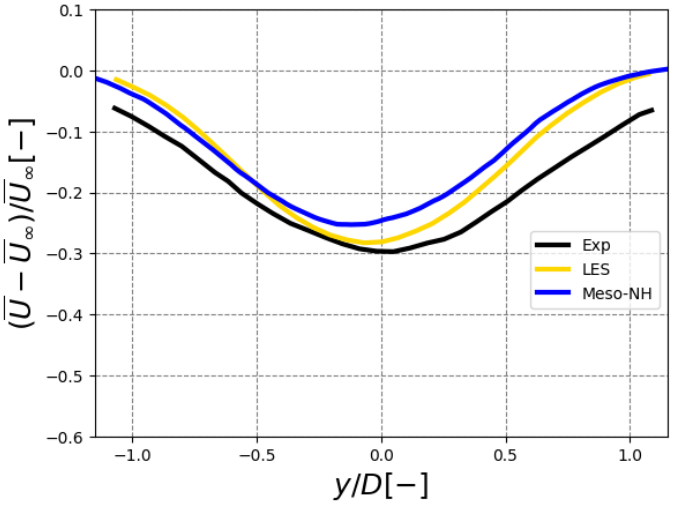

(d) Deficit at 5D downstream the wind turbine

Figure 8. Mean velocity deficit in the wake at hub height

7. Acknowledgment

We would like to thank Paula Doubrawa for her clarification on some points of the benchmark and for the data she provided. A special thank also to the Meso-NH support for their help on the model configuration and their help on the implementation of various functions.

References

[1] R. J. Barthelmie, K. Hansen, S. T. Frandsen, O. Rathmann, J. G. Schepers, W. Schlez, J. Phillips, K. Rados, A. Zervos, E. S. Politis, and P. K. Chaviaropoulos, "Modelling and measuring flow and wind turbine wakes in large wind farms offshore," *Wind Energy*, vol. 12, pp. 431–444, July 2009.

[2] F. Porté-Agel, M. Bastankhah, and S. Shamsoddin, "Wind-Turbine and Wind-Farm Flows: A Review," *Boundary-Layer Meteorology*, Sept. 2019.

[3] G. C. Larsen, H. Madsen Aagaard, F. Bingöl, J. Mann, S. Ott, J. N. Sørensen, V. Okulov, N. Troldborg, N. M. Nielsen, K. Thomsen, T. J. Larsen, and R. Mikkelsen, *Dynamic wake meandering modeling*. Risø National Laboratory, 2007.

[4] A. Neubert, "Windfarmer white paper," 2016.

[5] P.-A. Joulin, M. L. Mayol, V. Masson, F. Blondel, Q. Rodier, M. Cathelain, and C. Lac, "The actuator line method in the meteorological LES model meso-NH to analyze the horns rev 1 wind farm photo case," *Frontiers in Earth Science*, vol. 7, jan 2020.

[6] G. C. Larsen, H. A. Madsen, K. Thomsen, and T. J. Larsen, "Wake meandering: a pragmatic approach," *Wind Energy*, vol. 11, pp. 377–395, July 2008.

[7] S.-P. Breton, J. Sumner, J. N. Sørensen, K. S. Hansen, S. Sarmast, and S. Ivanell, "A survey of modelling methods for high-fidelity wind farm simulations using large eddy simulation," *Philosophical Transactions of the Royal Society A: Mathematical, Physical and Engineering Sciences*, vol. 375, p. 20160097, Mar. 2017.

[8] C. Lac, J.-P. Chaboureau, V. Masson, J.-P. Pinty, P. Tulet, J. Escobar, M. Leriche, C. Barthe, B. Aouizerats, C. Augros, P. Aumond, F. Auguste, P. Bechtold, S. Berthet, S. Bielli, F. Bosseur, O. Caumont, J.-M. Cohard, J. Colin, F. Couvreux, J. Cuxart, G. Delautier, T. Dauhut, V. Ducrocq, J.-B. Filippi, D. Gazen, O. Geoffroy, F. Gheusi, R. Honnert, J.-P. Lafore, C. L. Brossier, Q. Libois, T. Lunet, C. Mari, T. Maric, P. Mascart, M. Mogé, G. Molinié, O. Nuissier, F. Pantillon, P. Peyrillé, J. Pergaud, E. Perraud, J. Pianezze, J.-L. Redelsperger, D. Ricard, E. Richard, S. Riette, Q. Rodier, R. Schoetter, L. Seyfried, J. Stein, K. Suhre, M. Taufour, O. Thouron, S. Turner, A. Verrelle, B. Vié, F. Visentin, V. Vionnet, and P. Wautelet, "Overview of the meso-NH model version 5.4 and its applications," *Geoscientific Model Development*, vol. 11, pp. 1929–1969, may 2018.

[9] P. Doubrawa, E. W. Quon, L. A. Martinez-Tossas, K. Shaler, M. Debnath, N. Hamilton, T. G. Herges, D. Maniaci, C. L. Kelley, A. S. Hsieh, M. L. Blaylock, P. Laan, S. J. Andersen, S. Krueger, M. Cathelain, W. Schlez, J. Jonkman, E. Branlard, G. Steinfeld, S. Schmidt, F. Blondel, L. J. Lukassen, and P. Moriarty, "Multimodel validation of single wakes in neutral and stratified atmospheric conditions," *Wind Energy*, jul 2020.

[10] R. F. Mikkelsen, *Actuator Disc Methods Applied to Wind Turbines*. PhD Thesis, Technical University of Denmark, 2004.

[11] N. Troldborg, G. C. Larsen, H. A. Madsen, K. S. Hansen, J. N. Sørensen, and R. Mikkelsen, "Numerical simulations of wake interaction between two wind turbines at various inflow conditions," *Wind Energy*, vol. 14, pp. 859–876, Oct. 2010.

[12] J. P. Lafore, J. Stein, N. Asencio, P. Bougeault, V. Ducrocq, J. Duron, C. Fischer, P. Héreil, P. Mascart, V. Masson, J. P. Pinty, J. L. Redelsperger, E. Richard, and J. V.-G. de Arellano, "The meso-NH atmospheric simulation system. part i: adiabatic formulation and control simulations," *Annales Geophysicae*, vol. 16, no. 1, pp. 90–109, 1998.

[13] J. W. Deardorff, "Stratocumulus-capped mixed layers derived from a three-dimensional model," *Boundary-Layer Meteorology*, vol. 18, pp. 495–527, jun 1980.

[14] J. Stein, E. Richard, J. P. Lafore, J. P. Pinty, N. Asencio, and S. Cosma, "High-resolution non-hydrostatic simulations of flash-flood episodes with grid-nesting and ice-phase parameterization," *Meteorology and Atmospheric Physics*, vol. 72, pp. 203–221, feb 2000.

[15] P.-A. Joulin, *Modélisation à fine échelle des interactions entre parcs éoliens et météorologie locale*. PhD thesis, SDU2E, 2019. Thèse de doctorat dirigée par Masson, Valéry Océan, atmosphère, climat Toulouse, INPT 2019.

[16] H. Glauert, "Airplane Propellers," in *Aerodynamic Theory*, pp. 169–360, Springer Berlin Heidelberg, 1935.

[17] J. N. Sørensen and W. Z. Shen, "Numerical modeling of wind turbine wakes," *Journal of Fluids Engineering*, vol. 124, pp. 393–399, may 2002.

[18] P. Joulin, M. Mayol, F. Blondel, V. Masson, Q. Rodier, and C. Lac, "Coupling the actuator line method to the high order meteorological LES model meso-NH to study wind farm wakes impacts on local meteorology," *Journal of Physics: Conference Series*, vol. 1256, p. 012019, jul 2019.

[19] R. J. Stevens, L. A. Martínez-Tossas, and C. Meneveau, "Comparison of wind farm large eddy simulations using actuator disk and actuator line models with wind tunnel experiments," *Renewable Energy*, vol. 116, pp. 470–478, feb 2018.

[20] C. L. Kelley and B. L. Ennis, "SWiFT site atmospheric characterization," tech. rep., jan 2016.

[21] P. Doubrawa, M. Debnath, P. J. Moriarty, E. Branlard, T. G. Herges, D. C. Maniaci, and B. Naughton, "Benchmarks for model validation based on LiDAR wake measurements," *Journal of Physics: Conference Series*, vol. 1256, p. 012024, jul 2019.